

# Correlation Analyses on Binding Affinity of Substituted Benzenesulfonamides with Carbonic Anhydrase Using *ab Initio* MO Calculations on Their Complex Structures

Tatsusada Yoshida, Yohei Munei, Seiji Hitaoka, and Hiroshi Chuman\*

Institute of Health Biosciences, The University of Tokushima Graduate School, 1-78 Shomachi, Tokushima 770-8505, Japan

Received February 15, 2010

Quantitative structure–activity relationship analyses on the free energy change during complex formation between substituted benzenesulfonamides (BSAs) and bovine carbonic anhydrase II (bCA II) were performed using generalized Born/surface area (GB/SA) and *ab initio* fragment molecular orbital (FMO) calculations for the whole complex structures. The result shows that the overall free energy change is governed by the contribution from solvation and dissociation free energy changes accompanying by complex formation. The FMO–IFIE (interfragment interaction energy) analysis quantitatively revealed that the intrinsic interaction energy of bCA II with BSAs is mostly from interactions with amino acid residues in the active site of bCA II. The “Zn block” ( $\text{Zn}^{2+}$  and three histidine residues coordinated to  $\text{Zn}^{2+}$ ) in the active site shows the lowest interaction energy and the greatest variance of interaction energy with BSAs through their coordination interaction. The proposed procedure was demonstrated to provide a quantitative basis for understanding a ligand–protein interaction at electronic and atomic levels.

## 1. INTRODUCTION

The ubiquitous enzyme carbonic anhydrase (CA) is a zinc-containing metalloenzyme, which catalyzes a variety of physiological and physiopathological reactions such as the reversible hydration of carbon dioxide to the bicarbonate ion, aldehyde hydration, hydrolysis of alkyl and aryl esters, and urine formation. CA has been drawing much attention due to its catalytic mechanism in which a metal atom plays a critical role.<sup>1–3</sup>

In mammals, 12 CA isozymes (CA I–IV, VA, VB, VI, VII, IX, and XII–XIV), which exhibit catalytic activity as to the  $\text{CO}_2$  hydration reaction, with different catalytic activities, selectivities, subcellular localizations, and tissue distributions have been so far isolated. Many of these CA isozymes are important therapeutic targets to be inhibited for treating a range of disorders such as edema, glaucoma, epilepsy, obesity, osteoporosis, and cancer.<sup>4–10</sup>

The X-ray structures of CAs have shown that the zinc ion ( $\text{Zn}^{2+}$ ) within the active site is coordinated to three histidine residues and one water molecule (or hydroxide anion) and that the water molecule is replaced by a CA inhibitor as the fourth ligand of  $\text{Zn}^{2+}$ .<sup>11–17</sup>

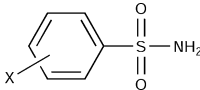
Most CA inhibitors contain an essential sulfonamide ( $\text{SO}_2\text{NH}_2$ ) group attached to an aromatic or heteroaromatic ring, as exemplified by the structures of clinically used drugs such as acetazolamide, ethoxzolamide, sulthiame, brinzolamide, indisulam, zonisamide, sulpiride, COUMATE, EMATE, celecoxib, and valdecoxib.<sup>10,18</sup> In 1969, Kakeya et al. performed QSAR (quantitative structure–activity relationship) analyses of a series of substituted benzenesulfonamides

(BSAs)<sup>19–22</sup> for bovine CA (denoted as bCA) inhibition (mixture of bCA I and bCA II). Since the appearance of Kakeya's pioneering work, a number of QSAR analyses of CA inhibitors involving various free-energy related descriptors, such as Hammett  $\sigma$ ,  $\log P$ ,  $\pi$ , quantum mechanical indices, and topological indexes, have been reported.<sup>23–36</sup> Comprehensive reviews of QSAR studies on CA inhibition have also been published.<sup>37,38</sup> In such QSAR analyses of BSAs, as reported by Kakeya et al.<sup>19,20</sup> and Hansch et al.,<sup>23,25</sup> the electronic descriptor Hammett  $\sigma$  was undoubtedly significant.

We have recently proposed a novel QSAR procedure where QSAR descriptors are derived from *ab initio* fragment molecular orbital (FMO) calculations for the whole structure of ligand–protein complex.<sup>39,40</sup> This procedure provides us with a quantitative and detailed picture and an understanding of the ligand–protein interaction at the atomic and electronic levels. The interaction energy and level of charge transfer between each amino acid residue in HIV-1 protease and an inhibitor are computable using *ab initio* FMO calculations, and these two quantum chemical quantities for a congeneric series of cyclic urea type HIV-1 protease inhibitors are both nicely correlated with the variation in the observed inhibitory potency.

In this work, we constructed complex structures of bCA II with a series of BSAs using molecular dynamics (MD) and QM/MM (hybrid quantum mechanical/molecular mechanical method) calculations. We assumed that the overall free energy change on the complex formation was expressed as the sum of the intrinsic interaction energy of a BSA with bCA II, the solvation free energy change, and dissociation free energy of a ligand, which were calculated with FMO, generalized Born/surface area (GB/SA), and GB/SA together

\* To whom correspondence should be addressed. Tel.: +81-88-633-7257. Fax: +81-88-633-9508. E-mail: hchuman@ph.tokushima-u.ac.jp.

**Table 1.** Chemical Structure of BSA, log  $K_i$ ,  $\Delta G$ , Hammett  $\sigma$ , and  $pK_a$ 


compound		log $K_i^a$	$\Delta G^b$	$pK_a^a$	$\sigma$
no.	X				
1	4-CH <sub>3</sub> NH	-4.96	-6.54	11.00	-0.840
2	4-NH <sub>2</sub>	-4.60	-6.07	10.48	-0.660
3	4-CH <sub>3</sub> O	-5.30	-6.99	10.17	-0.268
4	4-CH <sub>3</sub>	-5.49	-7.24	10.11	-0.170
5	3-CH <sub>3</sub>	-5.22	-6.88	10.06	-0.069
6	H	-5.12	-6.75	9.95	0.000
7	4-Cl	-5.96	-7.85	9.88	0.227
8	4-Br	-5.96	-7.85	9.87	0.232
9	3-Cl	-5.92	-7.80	9.80	0.373
10	4-CH <sub>3</sub> CO	-5.89	-7.76	9.66	0.502
11	4-CN	-6.19	-8.15	9.26	0.660
12	3-NO <sub>2</sub>	-6.12	-8.07	9.42	0.710
13	4-NO <sub>2</sub>	-6.26	-8.25	9.04	0.778
14	3,4-di-Cl	-6.52	-8.60	9.60	0.600
15	3-NO <sub>2</sub> , 4-Cl	-6.60	-8.70	9.34	0.937
16	3-CF <sub>3</sub> , 4-NO <sub>2</sub>	-6.66	-8.77	9.09	1.208

<sup>a</sup> Taken from ref 19. <sup>b</sup>  $\Delta G = RT \ln K_i$  ( $T = 288$  K), in kilocalories per mole.

with self-consistent reaction field (SCRf) calculations, respectively. The intrinsic interaction energy was further decomposed into contributions from each amino acid residue in bCA II (IFIE terms) by FMO-IFIE analyses. Correlations between the total intrinsic interaction energy and IFIE terms were examined to understand the critical interaction that governs the variation of the intrinsic affinity of BSAs with bCA II. Finally, we discuss the relation of Hammett  $\sigma$  with the overall and intrinsic interaction energies.

## 2. METHODS

**2.1. Compound Set.** The structure-activity data for the series of BSAs used in the present study were taken from the publication reported by Kakeya et al.<sup>19</sup> BSAs in the compound set have a relatively small size of substituents at the para, meta, and ortho positions in the benzene ring. From the original compound set, we selected the 16 para- and meta-substituted compounds listed in Table 1, because ortho-substituted compounds often show extra substituent effects, probably due to the steric interaction on the binding with a protein, and are often treated as outliers in QSAR analyses. The inhibitory equilibrium constant  $K_i$  value was also taken from those reported by Kakeya et al. (values at 15 °C). Table 1 lists the log  $K_i$ , the overall free energy change on the complex formation  $\Delta G$  ( $=2.303RT \log K_i$ ),  $pK_a$ , and Hammett  $\sigma$  values for the compounds examined in this study.

**2.2. Active Form of BSAs in Complex with bCA II.** Although there has been controversy on the sulfonamide inhibition mechanism whether the active form during complex formation is the ionized (anion, R-SO<sub>2</sub>NH<sup>-</sup>) or neutral (R-SO<sub>2</sub>NH<sub>2</sub>) form of sulfonamides, the following experimental results a-c have been reported. (a) Lindskog and Thorslund<sup>41</sup> showed that the complex formation is pH dependent and proposed the formation occurs through a direct reaction of the ionized sulfonamide with bovine cobalt CA II from the rate and equilibrium data. (b) Kanamori and Roberts<sup>42</sup> showed that the sulfonamide moiety in the complex

state is negatively ionized from the measurement of the <sup>15</sup>N-<sup>1</sup>H coupling constant in <sup>15</sup>N NMR. Blackburn et al.<sup>43</sup> also proposed the ionized mechanism from the fact that the proton-coupled <sup>15</sup>N resonance of the CA (mixture of bCA I and bCA II)-bound BSA exhibits a multiplet pattern. The multiplicity of the signal can be explained by the loss of one proton from nitrogen in the sulfonamide on binding to the enzyme active site. These results strongly indicated that a BSA is bound as its ionized form. (c) The crystallographic and titration studies on a model (macrocyclic triamines) for sulfonamide inhibition of CA, reported by Koike et al.,<sup>44</sup> clearly revealed that the sulfonamide hydrogen can be dissociated at pH as low as ~8 to bind Zn<sup>2+</sup> and that deprotonated sulfonamide inhibitors bind with Zn<sup>2+</sup> at physiological pH. Although the possibility of the protonated sulfonamides as the binding form cannot be ruled out completely, the above experimental results strongly support that BSAs take their ionized form in the complex with CA II. In addition, Krishnamurthy et al.<sup>45,46</sup> recently proposed the replacement of H<sub>2</sub>O in the [CA II-Zn<sup>2+</sup>-H<sub>2</sub>O] complex with a BSA anion as the most likely mechanism. As to molecular calculations of the interaction energy between CA II and a BSA, Merz et al.<sup>47</sup> demonstrated that the experimental binding free energy difference ( $\Delta\Delta G_{\text{bind}}$ ) between two BSAs with different substituents on the benzene ring is nicely reproducible with free energy perturbation simulations, on the assumption that they bind with human CA II (hCA II) in their anionic form. For these reasons, we dealt with a complex structure between an ionized (anion) BSA and bCA II in the following calculations.

**2.3. Linear Expression of the Overall Free Energy Change during Complex Formation.** A basic assumption when dissecting free energy terms is that they are all additive.<sup>48-51</sup>  $\Delta G$  in eq 1a is the overall free energy change obtained from the experimentally determined inhibitory constant  $K_i$ ;  $\Delta G = 2.303RT \log K_i$ .

$$\Delta G = \Delta G_{\text{bind}} + \Delta G_{\text{sol}} + \Delta G_{\text{dis}} + \Delta G_{\text{others}} \quad (1a)$$

$\Delta G_{\text{dis}}$  and  $(\Delta G_{\text{bind}} + \Delta G_{\text{sol}})$  represent free energy changes in the dissociation ( $\text{BSA}(-\text{SO}_2\text{NH}_2) + \text{H}_2\text{O} \leftrightarrow \text{BSA}(-\text{SO}_2\text{NH}^-) + \text{H}_3\text{O}^+$ ) and binding ( $\text{CA II-Zn}^{2+} - \text{H}_2\text{O} + (-\text{NHSO}_2-)\text{BSA} \leftrightarrow \text{CA II-Zn}^{2+} - (-\text{NHSO}_2-)\text{BSA} + \text{H}_2\text{O}$ ) processes, respectively.  $\Delta G_{\text{bind}}$  is the intrinsic interaction energy between a BSA and bCA II. It should be noted that  $\Delta G_{\text{bind}}$  in eq 1a does not include the solvation and dissociation free energy contributions.  $\Delta G_{\text{sol}}$  and  $\Delta G_{\text{dis}}$  are the solvation and dissociation free energy changes, respectively.  $\Delta G_{\text{others}}$  is the sum of the free energy terms other than  $\Delta G_{\text{bind}}$ ,  $\Delta G_{\text{sol}}$ , and  $\Delta G_{\text{dis}}$ .  $\Delta G_{\text{others}}$  includes energy terms such as the deformation energy of a protein<sup>52,53</sup> and the ionization energy of a buffer system.<sup>54,55</sup>

In the complex formation of a series of congeneric ligands with their target protein, "a penalty energy term"  $\Delta G_{\text{others}}$  is considered to be a positive constant or linearly correlated with  $(\Delta G_{\text{bind}} + \Delta G_{\text{sol}} + \Delta G_{\text{dis}})$  (i.e.,  $\Delta G_{\text{others}} = \beta (\Delta G_{\text{bind}} + \Delta G_{\text{sol}} + \Delta G_{\text{dis}}) + \text{constant}$ ;  $\beta < 0$ ).

$$\Delta G = (1 + \beta)(\Delta G_{\text{bind}} + \Delta G_{\text{sol}} + \Delta G_{\text{dis}}) + \text{constant} \quad (1b)$$

Equation 1b could be considered to be a primitive scoring function that scores protein-ligand binding affinities. A





active sites of hCA II and bCA II (e.g., Ile90 and Val90, Val133 and Ala133, respectively), 52 amino acid residues in total are different in their sequences. We decided to use the X-ray coordinates of 1V9I as the initial structure for modeling, because the activity value used in this work was the inhibitory potency ( $\log K_i$ ) as to bCA (mixture of bCA I and bCA II). The crystallographic structure of bCA I is not known at present. However, it can be reasonably assumed that the structure of bCA I is very similar with that of bCA II, because the sequence similarity between them reaches 84%. Probably amino acid residues in the active site are highly conserved in the two proteins. Therefore, we started to construct the initial structure of the complex of the unsubstituted BSA ( $X = H$ , compound **6**) with bCA II using the coordinates of 1V9I. The mutated amino acid residue Cys253 in 1V9I was replaced by Gln253 in the wild-type bCA II, and then hydrogen atoms were added. We assumed ionized forms for residues Arg, Lys, Asp, and Glu with ionizable side chains. Two sodium ions were added as counterions to neutralize the total  $-2$  charge of the bCA II–BSA complex. The bCA II–BSA complex was then solvated in a truncated octahedral box of TIP3P water extending 15 Å from the protein atom (10963 water molecules were added in total).

We adopted the bonded approach<sup>75,76</sup> for the molecular mechanics (MM) calculations to represent the Zn-coordination environment, placing explicit bonds between the zinc atom ( $Zn^{2+}$ ) and His93, His95, His118, and the BSA ( $X = H$ , compound **6**) coordinated to  $Zn^{2+}$ . Because the force field parameters around  $Zn^{2+}$  are unavailable for the standard AMBER force field, we derived these parameters from ab initio MO calculations (Gaussian03 program<sup>77</sup>) for the model complex ( $[Zn^{2+}(\text{methylimidazole})_3(BSA^-)]^+$ ) shown in Table 2. According to the procedure suggested by Merz and his co-workers,<sup>78,79</sup> equilibrium bond lengths and angles involving  $Zn^{2+}$  were derived from the HF/6-31G\* optimized structure of the model. The bond stretching and angle bending force constants were taken from those reported by Merz et al.<sup>47</sup> All the torsional parameters around  $Zn^{2+}$  were set to zero.<sup>75</sup> The RESP (restrained electrostatic potential) charges<sup>80</sup> for MM and MD calculations were determined at the DFT/B3LYP level of theory with the 6-31G\* basis set for the H, C, N, O, and S atoms, and LanL2DZ for the Zn atom. After small adjustments of the force constants, the modified force field calculation well-reproduced the HF/6-31G\* optimized structure of the model. The force constants and RESP charges determined for the model are summarized in Table 2.

MM and MD calculations for the complex structure were carried out using the AMBER 10 package<sup>81</sup> with parm99, and the modified parameters for the BSA (compound **6**),  $Zn^{2+}$ , His93, His95, and His118. Before MD runs, the system was energy-minimized to remove ill van der Waals contacts in the initial geometry. After energy minimization, the solvent molecules and counterions were initially relaxed by means of 100 ps of MD, keeping the solute (bCA II and compound **6**) fixed, and then the system was gradually heated to 300 K over a period of 100 ps. The equilibration MD of the system was performed at 300 K for 500 ps, at which point the energy of the system attained complete stability. The production run was carried out for 4.0 ns under the *NPT* conditions (1.0 atm, 300 K). The SHAKE algorithm<sup>82</sup> was employed to

restrain all bond lengths involving hydrogen atoms, and the time step for integration was set at 1.0 fs. A nonbonded energy cutoff distance of 8.0 Å was used, whereas the particle–mesh–Ewald (PME) method<sup>83</sup> was applied to include the contributions of long-range electrostatic interactions.

Snapshot structures of the bCA II–BSA (compound **6**) complex were collected from the MD trajectory over the 4.0 ns production run at 0.4 ps intervals (10000 snapshots in total). All the snapshots were clustered into five groups by means of the K-means method<sup>84</sup> based on root mean square deviation (rmsd) values for conformational differences in order to extract the representative MD structure that has the minimal sum of the squared displacements from other structures in the cluster with the largest population. The rmsd values of interatomic distances for all pairs of 10000 snapshots were calculated among the zinc atom, heavy atoms in the BSA (compound **6**), and  $C_\alpha$  atoms of the 21 amino acid residues in the BSA binding site (Ser28, Asn61, His63, Asn66, Gln91, His93, His95, Glu105, His118, Val120, Val141, Ser195–Leu202, Val205, and Trp207). The representative structure was energetically optimized, and then the resulting structure was used for the subsequent ONIOM calculations.

Other complex structures of bCA II with compounds **1–5** and **7–16**, i.e., other than **6**, were constructed by replacing the H atom in compound **6** with non-hydrogen substituents.

**2.5. Refinement of Complex Structures by ONIOM.** For further refinement of the complex structures of bCA II with BSAs (compounds **1–16**), we carried out QM/MM (quantum mechanics/molecular mechanics) geometry optimization with a two-layer ONIOM scheme<sup>85–87</sup> using the electronic embedding method<sup>88</sup> implemented in the Gaussian03 program.<sup>77</sup> The complex structure was divided into two layers, high-level and low-level layers, which were treated at the HF/6-31G\* level and with the AMBER parm99 force field, respectively. The zinc ion, a BSA, and the side-chain atoms of His93, His95, and His118 were taken for the high-level layer. The structure in the high-level layer was optimized, while atoms in the low layer were fixed.

Careful comparison of several X-ray complex structures comprising CA II and aromatic compounds having a sulfonamide group<sup>17,89</sup> showed that there are no water molecules inside the active site. Therefore, the complex structures without water molecules were used in the ONIOM and subsequent FMO calculations.

**2.6. Solvation and Dissociation Free Energies.** The solvation free energy change accompanied by complex formation ( $\Delta G_{\text{sol}} = G_{\text{sol}}(\text{complex}) - [G_{\text{sol}}(\text{bCA II}) + G_{\text{sol}}(\text{BSA}^-)]$ ) was calculated using the GB/SA (generalized Born/surface area) solvation model.<sup>90</sup> In a GB/SA calculation, the solvation free energy term ( $G_{\text{sol}}$ ) is expressed as the sum of electrostatic ( $G_{\text{ele}}$ ) and nonpolar ( $G_{\text{nonpolar}}$ ) contributions, and  $G_{\text{sol}}$  was calculated using the AMBER 10 package with a parm99 force field. For the electrostatic contribution, the dielectric constants of 1 and 80 were used for the interior and exterior of the solutes, respectively, with the RESP charge (calculated with B3LYP/6-31G(d)) assigned for each atom in a BSA. The nonpolar contribution was calculated as  $G_{\text{nonpolar}} = \gamma \text{SASA}$  (SASA = solvent accessible surface area) with  $\gamma = 0.0072$  (kcal/mol)·Å<sup>2</sup>.

The process of dissociation of a BSA into its anion (BSA<sup>−</sup>) was modeled as  $\text{BSA} + \text{H}_2\text{O} \leftrightarrow \text{BSA}^- + \text{H}_3\text{O}^+$

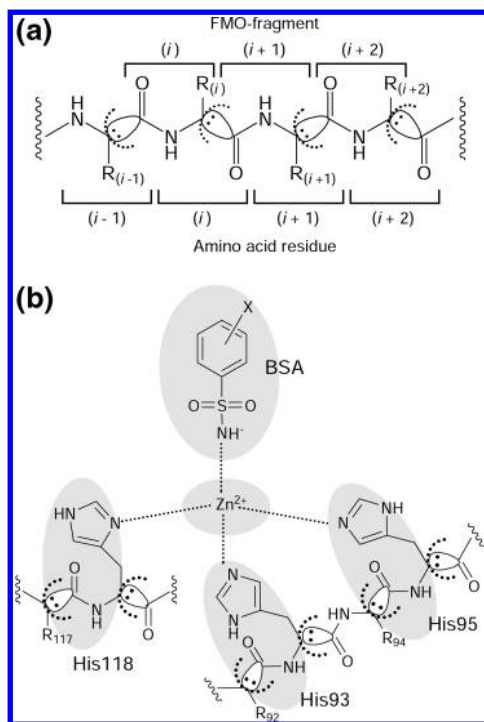


**Figure 1.** Fragmentation of polypeptides in FMO: (a) for peptides other than the Zn coordination environment. It should be noted that the definition of FMO fragment slightly differs from the standard notation of the amino acid residues; (b) for the Zn coordination environment. Atoms within dark areas are combined together and treated as a single FMO fragment (BSA–Zn and Zn blocks) in FMO calculations.

and the dissociation free energy ( $\Delta G_{\text{dis}}$ ) was defined as  $\Delta G_{\text{dis}} = [G_{\text{sol}}(\text{BSA}^-) + G_{\text{sol}}(\text{H}_3\text{O}^+)] - [G_{\text{sol}}(\text{BSA}) + G_{\text{sol}}(\text{H}_2\text{O})]$ , where  $G_{\text{sol}}$  represents the sum of the solvation ( $G_{\text{sol}}$ ) and internal electronic ( $E_{\text{vacuum}}$ ) energies.  $G_{\text{sol}}$  was estimated independently using the SCRf–CPCM model<sup>91</sup> (self-consistent reaction field–conductor-like polarizable continuum model combined with B3LYP/6-31+G(d,p)) and the GB/SA model under the same conditions as those used for calculation of the solvation free energy change.  $E_{\text{vacuum}}$  was calculated with MO calculations (B3LYP/6-31+G(d,p)). In a CPCM calculation, the scaled atomic radii were set as the default values implemented in Gaussian03.<sup>92</sup> Although the calculated  $\Delta G_{\text{dis}}$  value based on the above model is unreliable, the relative value ( $\Delta\Delta G_{\text{dis}}$ ) is usable for the quantitative estimation of free energy differences between a series of dissociation processes.<sup>93,94</sup> The geometries of BSAs and bCA II used in the GB/SA and CPCM calculations were those in the complex without relaxation.

**2.7. Ab Initio Fragment Molecular Orbital Calculations.** After the structural refinement by ONIOM, FMO calculations<sup>70</sup> were performed for the structures of 16 bCA II–BSA complexes and those without BSA. The FMO method divides a large biomolecular system into a collection of small FMO fragments. Figure 1a shows the FMO fragmentation for a polypeptide. In the present FMO calculations, as shown in Figure 1b, the Zn block (Zn<sup>2+</sup>, His93, His95, and His118) and a BSA were combined and treated as a single FMO fragment (BSA–Zn block)<sup>95</sup> to avoid the convergence problem in achieving SCF (self-consistent field). Similarly, for the calculation for a protein (without BSA), the Zn block

**Table 3.** Interatomic Distances (Å) and Angles (deg) between Unsubstituted BSA and Amino Acid Residues in the Active Site of CA II

(a) Geometry for the Zinc Environment				
distance <sup>a</sup>		calculated <sup>b</sup>	observed (X-ray) <sup>c</sup>	
r1	BSA–N···Zn	1.98	1.95	
r2	His93–Nε2···Zn	2.09	2.07	
r3	His95–Nε2···Zn	2.08	2.06	
r4	His118–Nδ1···Zn	2.09	2.10	

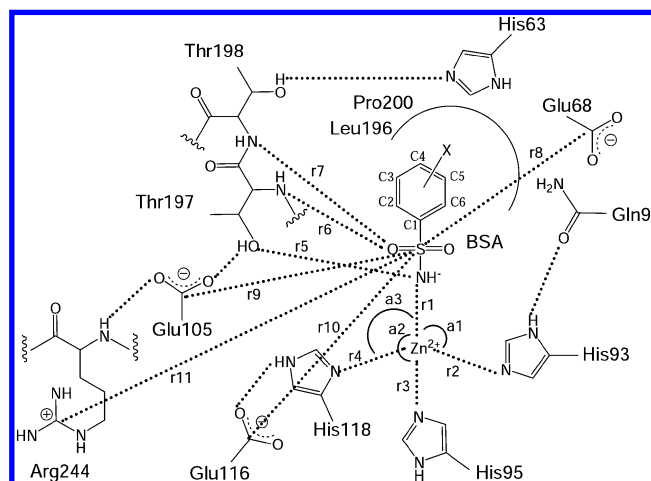
  

angle <sup>a</sup>		calculated <sup>b</sup>	observed (X-ray) <sup>c</sup>	
a1	BSA–N···Zn···Nε2–His93	112.2	112.2	
a2	BSA–N···Zn···Nε2–His95	103.5	114.7	
a3	BSA–N···Zn···Nδ1–His118	119.7	115.1	

(b) Interatomic Distances between BSA and Amino Acid Residues				
distance <sup>a</sup>		calculated <sup>b</sup>	observed (X-ray) <sup>c</sup>	
r5	BSA–N···Oγ1–Thr197	2.92	2.87	
r6	BSA–O···N–Thr197	2.87	2.97	
r7	BSA–O···N–Thr198	4.75	4.78	
r8	BSA–S···Cδ–Glu68	14.72	14.19	
r9	BSA–S···Cδ–Glu105	6.82	6.59	
r10	BSA–S···Cδ–Glu116	9.31	8.85	
r11	BSA–S···Cζ–Arg244	10.25	10.58	

<sup>a</sup> See Figure 2. <sup>b</sup> bCA II–compound **6** complex. <sup>c</sup> Complex structure of hCA II with compound **6** at 1.45 Å resolution (PDB code: 2WEJ).



**Figure 2.** BSA and amino acid residues in the active site of bCA II.

was treated as a single FMO fragment. For FMO fragments other than the BSA–Zn and Zn blocks, each FMO fragment consisted of a (–CO–NH–C<sub>α</sub>R–) unit, as shown in Figure 1a. FMO single-point energy calculations for the 16 complex structures were carried out at the HF/6-31G level with the ABINIT-MP program.<sup>96</sup>

The intrinsic interaction energy ( $\Delta E_{\text{bind}}$ ) between a BSA and bCA II is defined as  $\Delta E_{\text{bind}} = E(\text{complex}) - [E(\text{bCA II}) + E(\text{BSA}(-\text{SO}_2\text{NH}^-))]$ , and  $\Delta E_{\text{bind}}$  was estimated with FMO calculations.

**2.8. Interfragment Interaction Energy Difference (IFIED) Term.** The interfragment interaction energy (IFIE) is one of the most advantageous outcomes directly obtained with the FMO procedure, and analyses using IFIEs among the FMO fragments in a complex provide

**Table 4.**  $\Delta G$ ,  $\Delta E_{\text{bind}}$ ,  $\Delta G_{\text{sol}}$ , and  $\Delta G_{\text{dis}}$  Values

compound		$\Delta G^a$			$\Delta E_{\text{bind}}^a$	$\Delta G_{\text{sol}}^{a,e}$	$\Delta G_{\text{dis}}^{a,b}$	
no.	X	obsd	calcd <sup>c</sup>	calcd <sup>d</sup>			CPCM	GB/SA-MO
1	4-CH <sub>3</sub> NH	-6.54	-6.18	-6.18	-120.49	4.11	2.96	3.59
2	4-NH <sub>2</sub>	-6.07	-6.21	-6.46	-120.40	4.45	2.46	1.78
3	4-CH <sub>3</sub> O	-6.99	-6.90	-6.72	-116.46	1.30	0.82	2.22
4	4-CH <sub>3</sub>	-7.24	-7.16	-7.05	-116.64	0.46	0.41	1.41
5	3-CH <sub>3</sub>	-6.88	-6.99	-7.08	-115.34	1.18	0.12	0.07
6	H	-6.75	-7.30	-7.37	-116.09	0.00	0.00	0.00
7	4-Cl	-7.85	-7.87	-7.87	-112.15	-3.25	-0.94	-0.77
8	4-Br	-7.85	-7.95	-8.08	-111.95	-3.70	-0.96	-1.44
9	3-Cl	-7.80	-7.79	-7.83	-111.66	-2.66	-1.33	-1.27
10	4-CH <sub>3</sub> CO	-7.76	-7.90	-7.73	-112.24	-2.46	-1.84	-0.78
11	4-CN	-8.15	-8.44	-8.57	-108.92	-5.58	-2.59	-3.18
12	3-NO <sub>2</sub>	-8.07	-7.96	-7.93	-111.14	-2.26	-2.76	-2.41
13	4-NO <sub>2</sub>	-8.25	-8.42	-8.32	-109.52	-4.29	-3.53	-2.95
14	3,4-di-Cl	-8.60	-8.23	-8.22	-108.37	-5.29	-2.02	-1.87
15	3-NO <sub>2</sub> , 4-Cl	-8.70	-8.25	-8.24	-109.50	-3.56	-3.45	-3.31
16	3-CF <sub>3</sub> , 4-NO <sub>2</sub>	-8.77	-8.72	-8.64	-105.95	-5.71	-4.87	-4.45

<sup>a</sup> In kilocalories per mole. <sup>b</sup> Relative value from  $\Delta G_{\text{dis}}(\text{X} = \text{H})$ ,  $\Delta G_{\text{dis}}(\text{X} = \text{H}) = 51.44$  kcal/mol (CPCM),  $= -4.92$  kcal/mol (GB/SA-MO).

<sup>c</sup> Calculated from eq 4a in Table 5. <sup>d</sup> Calculated from eq 4b in Table 5. <sup>e</sup> Relative value from  $\Delta G_{\text{sol}}(\text{X} = \text{H})$ ,  $\Delta G_{\text{sol}}(\text{X} = \text{H}) = 74.53$  kcal/mol.

detailed information on the interaction between a ligand and protein.<sup>39,40</sup> We previously demonstrated that the total interaction energy between a protein and its ligand (i.e., binding energy  $\Delta E_{\text{bind}}$ ) is approximately but nicely given the sum of the IFIE of the ligand fragment with amino acid residue fragments (FMO fragments) in the protein ( $\Sigma \text{IFIE}(i)$ ).<sup>39,40</sup>

In the present study, it is impossible to directly determine the IFIE(*i*) values of a BSA with FMO fragments including the Zn block in bCA II, because a BSA and the Zn block were allocated to the same fragment in the FMO calculations. From the original formulation of the FMO theory with reasonable approximations, we newly defined IFIED(*i*) to estimate the interaction energy of a BSA with the *i*th fragment except without the Zn block in bCA II:

$$\text{IFIED}(i) = \text{IFIE}_{\text{complex}}(i) - \text{IFIE}_{\text{apo}}(i) \quad (2)$$

where  $\text{IFIE}_{\text{complex}}(i)$  and  $\text{IFIE}_{\text{apo}}(i)$  are the IFIEs of the *i*th fragment with the BSA-Zn and Zn blocks, respectively. IFIED(Zn block) was estimated separately from the supermolecule calculation for the same model ( $[\text{Zn}^{2+}(\text{methylimidazole})_3(\text{BSA}^-)]^+$ ) used for determining the RESP charges for the MM and MD calculations ( $\text{IFIED}(\text{Zn block}) = E([\text{Zn}^{2+}(\text{methylimidazole})_3(\text{BSA}^-)]^+) - E([\text{Zn}^{2+}(\text{methylimidazole})_3]^{2+}) - E(\text{BSA}^-)$ ).

### 3. RESULTS AND DISCUSSION

**3.1. bCA II-BSA Complex Structures.** The complex structures of bCA II with 16 BSAs were optimized with the MD-MM procedure and further refined using ONIOM calculations. The ONIOM optimized structures nicely reproduced the experimental distorted tetrahedral geometry for the Zn-coordination environment. Table 3a lists the optimized geometries of compound **6** (unsubstituted BSA) around the Zn ion, compared with those of the X-ray crystallographic structure of the hCA II-compound **6** complex.<sup>17</sup> The calculated distances between the Zn ion and the three nitrogen atoms at His93, His95, and His118 are between 2.08 and 2.09 Å (experimental values, 2.06 and 2.10 Å), and that between the Zn atom and the

nitrogen atom of the sulfonamide group ( $\text{SO}_2\text{NH}^-$ ) in BSA is 1.98 Å (1.95 Å). These results indicate that the nitrogen atom of the sulfonamide group more tightly coordinates to the Zn ion than the three nitrogen atoms in His93, His95, and His118. The calculated angles are also in agreement with the experimental ones within a difference of 15°. The 16 complex structures after the ONIOM optimization were used for the subsequent QSAR analyses. Table 3b lists the interatomic distances represented by dotted lines in Figure 2, where a BSA, the Zn block, and amino acid residues in the active site of bCA II are schematically shown. The calculated distances from the sulfonamide group to the amino acid residues shown in Figure 2 nicely agree with the corresponding observed ones in the hCA II-unsubstituted BSA complex.

**3.2. Contribution of the Intrinsic Interaction Energy to the Complex Formation.** Table 4 lists the overall free energy change  $\Delta G$ , the intrinsic interaction energy  $\Delta E_{\text{bind}}$ , the solvation free energy change  $\Delta G_{\text{sol}}$ , and the dissociation free energy  $\Delta G_{\text{dis}}$  values. A nice linearity between  $\Delta G$  and ( $\Delta G_{\text{sol}} + \Delta G_{\text{dis}}$ ) was confirmed by eqs 3a and 3b (summarized in Table 5 along with eqs 4a, 4b, 5a, 5b, and 6). Assuming  $\alpha_{\text{bind}} = 0.65$  with the calculated  $\Delta E_{\text{bind}}$ ,  $\Delta G_{\text{sol}}$ , and  $\Delta G_{\text{dis}}$  values, eq 1d gives eqs 4a and 4b. The coefficients of  $[(1 - \alpha_{\text{bind}})\Delta E_{\text{bind}} + \Delta G_{\text{sol}} + \Delta G_{\text{dis}}]$  and intercepts are very similar to each other in eqs 4a and 4b, which differ in the means of estimation of  $\Delta G_{\text{dis}}$ .  $\beta$  in eq 1d is now estimated to be  $\sim -0.80$  from eqs 4a and 4b. As expected, a negative value of  $\beta$  indicates that  $\Delta G_{\text{others}}$  in eq 1d acts as “a penalty energy term”. Although  $\alpha_{\text{bind}}$  was tentatively taken to be 0.65 when formulating eqs 4a and 4b, variation of  $\alpha_{\text{bind}}$  between 0.35 and 0.95 ( $0.65 \pm 0.30$ ) did not cause very significant changes in the  $\beta$  value or correlation coefficient  $r$ ;  $\beta = -0.707$  to  $-0.847$ ,  $r = 0.931$  to  $0.957$  and  $\beta = -0.731$  to  $-0.852$ ,  $r = 0.890$  to  $0.940$  with eqs 4a and 4b, respectively.

Equations 5a and 5b show that there is a nearly perfect anticorrelation ( $r \geq 0.985$ ) between  $\Delta E_{\text{bind}}$  and ( $\Delta G_{\text{sol}} + \Delta G_{\text{dis}}$ ), suggesting that the intrinsic interaction energy ( $\Delta E_{\text{bind}}$ ) and the sum of the solvation and dissociation energies  $[(\Delta G_{\text{sol}} + \Delta G_{\text{dis}})]$  exhibit opposite correlations with the overall free energy change ( $\Delta G$ ), as confirmed

**Table 5.** Correlation Equations

$Y = aX + \text{constant} \quad (n = 16)$			$\Delta G_{\text{dis}}$	$a^a$	constant <sup>a</sup>	$r^b$	$s^c$	$s_{\text{cv}}^d$	$F^e$
eq no.	$Y$	$X$							
3a	$\Delta G$	$\Delta G_{\text{sol}} + \Delta G_{\text{dis}}$	CPCM	$0.147 \pm 0.0252$	$-7.23 \pm 0.147$	0.958	0.241	0.264	157
3b	$\Delta G$	$\Delta G_{\text{sol}} + \Delta G_{\text{dis}}$	GB/SA-MO	$0.142 \pm 0.0291$	$-7.28 \pm 0.169$	0.942	0.283	0.312	110
4a <sup>f</sup>	$\Delta G$	$(1 - \alpha_{\text{bind}})\Delta E_{\text{bind}} + \Delta G_{\text{sol}} + \Delta G_{\text{dis}}$	CPCM	$0.202 \pm 0.0378$	$0.908 \pm 1.61$	0.951	0.261	0.284	131
4b <sup>f</sup>	$\Delta G$	$(1 - \alpha_{\text{bind}})\Delta E_{\text{bind}} + \Delta G_{\text{sol}} + \Delta G_{\text{dis}}$	GB/SA-MO	$0.192 \pm 0.0449$	$0.441 \pm 1.90$	0.926	0.318	0.349	84.2
5a	$\Delta E_{\text{bind}}$	$\Delta G_{\text{sol}} + \Delta G_{\text{dis}}$	CPCM	$-0.795 \pm 0.0638$	$-115 \pm 0.373$	0.990	0.610	0.647	715
5b	$\Delta E_{\text{bind}}$	$\Delta G_{\text{sol}} + \Delta G_{\text{dis}}$	GB/SA-MO	$-0.779 \pm 0.0770$	$-115 \pm 0.446$	0.985	0.748	0.811	470
6	$\Delta G$	$\Delta E_{\text{bind}}$		$-0.185 \pm 0.0288$	$-28.5 \pm 3.26$	0.965	0.221	0.243	188

<sup>a</sup> Plus/minus values are the 95% confidence intervals. <sup>b</sup> Correlation coefficient. <sup>c</sup> Standard deviation. <sup>d</sup> Standard deviation of cross-validated (leave-one-out) prediction. <sup>e</sup> Ratio of regression and residual variances. <sup>f</sup>  $\alpha_{\text{bind}} = 0.65$ .

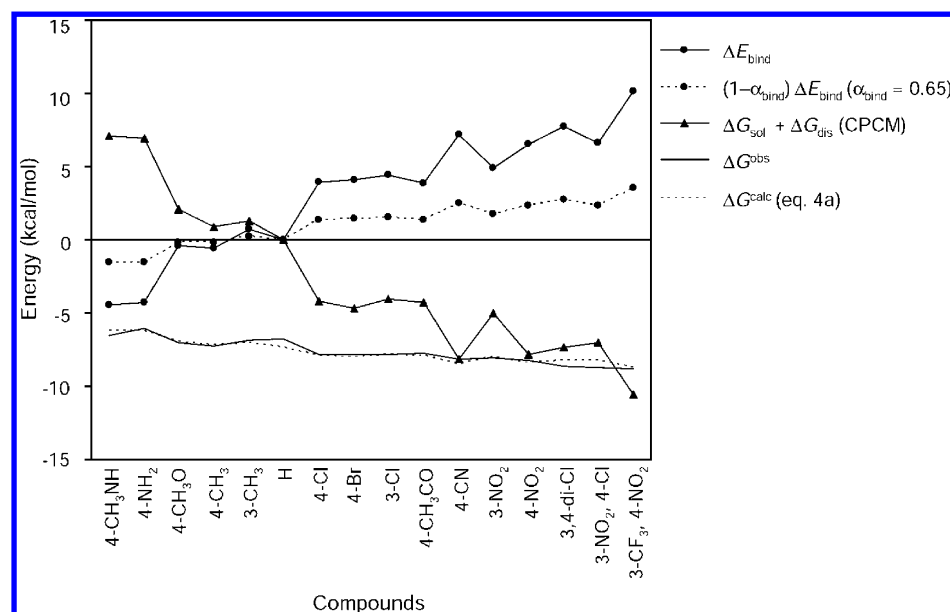


**Figure 3.** Variations in  $\Delta G_{\text{sol}} + \Delta G_{\text{dis}}$ ,  $\Delta E_{\text{bind}}$ , and  $\Delta G$  values.  $\Delta G_{\text{sol}} + \Delta G_{\text{dis}}$  and  $\Delta E_{\text{bind}}$  are the relative energies from those for the complex of bCA II with the unsubstituted BSA ( $X = \text{H}$ ), respectively.

by eqs 6 and 3a (3b), respectively. The coefficient value of  $\Delta E_{\text{bind}}$  in eq 1d is  $(1 - \alpha_{\text{bind}})$  times smaller than that of  $(\Delta G_{\text{sol}} + \Delta G_{\text{dis}})$ . These results suggest that the relative contribution from the solvation and dissociation free energies overwhelms that from the intrinsic interaction energy and that it governs the overall free energy change, as can be seen in Figure 3. As expected, the correlation coefficients between  $\text{p}K_{\text{a}}$  and  $\Delta G_{\text{dis}}$  were 0.972 (CPCM) and 0.953 (GB/SA-MO).

Although the contribution of the sum of the solvation and dissociation free energies plays a decisive role in determination of the overall free energy change, quantitative analysis of the intrinsic interaction energy between BSAs and bCA II is of essential importance for understanding the interaction mechanism in detail at the atomic and electronic levels. In the next section, we discuss the results regarding the intrinsic interaction energy ( $\Delta E_{\text{bind}}$ ) using IFIED analyses.

**3.3. Decomposition of the Intrinsic Interaction Energy into Interaction Energies with Individual Amino Acid Residues in bCA II.** To clarify the quantitative contribution of each amino acid residue (FMO fragment) to the intrinsic interaction energy  $\Delta E_{\text{bind}}$ , we calculated IFIED( $i$ ), which represents the interaction energy for a BSA with the  $i$ th FMO fragment (including the Zn block) in bCA

II. Figure 4a shows the IFIED( $i$ ) values of all the 257 FMO fragments in the complex of bCA II with compound **6** ( $X = \text{H}$ ). Figure 4b shows the differences between IFIED( $i$ ) values calculated with HF/6-31G and those with MP2/6-31G for the complex with compound **6**. Although the difference (MP2/6-31G – HF/6-31G) is  $-28.6$  kcal/mol, Figure 4b shows that the difference between the IFIED values of each FMO fragment is very small ( $-0.03$  kcal/mol on average) except those of FMO fragments Leu196 ( $-6.52$ ), Thr197 ( $-4.59$ ), Thr198 ( $-2.88$ ), and the Zn block ( $-8.01$ ). The difference between the two IFIED values of the above FMO fragments is expected to behave linearly or constantly for the 16 complexes.<sup>97</sup> Therefore, we used the results for HF/6-31G calculations in the following analyses.

Equation 7 (listed in Table 6 along with eqs 8 and 9) shows that  $\Sigma\text{IFIED}(i)$  is nicely correlated with  $\Delta E_{\text{bind}}$ . It should be noted that the slope of  $\Sigma\text{IFIED}(i)$  in eq 7 is close to unity, indicating that the change in  $\Sigma\text{IFIED}(i)$  is nearly equal to that in  $\Delta E_{\text{bind}}$ .

Most of peaks with a large absolute IFIED value in Figure 4a are due to the electrostatic interactions between a negatively charged BSA and charged FMO fragments closely located around the active pocket; negatively charged FMO fragments (Asp and Glu) exhibit repulsive



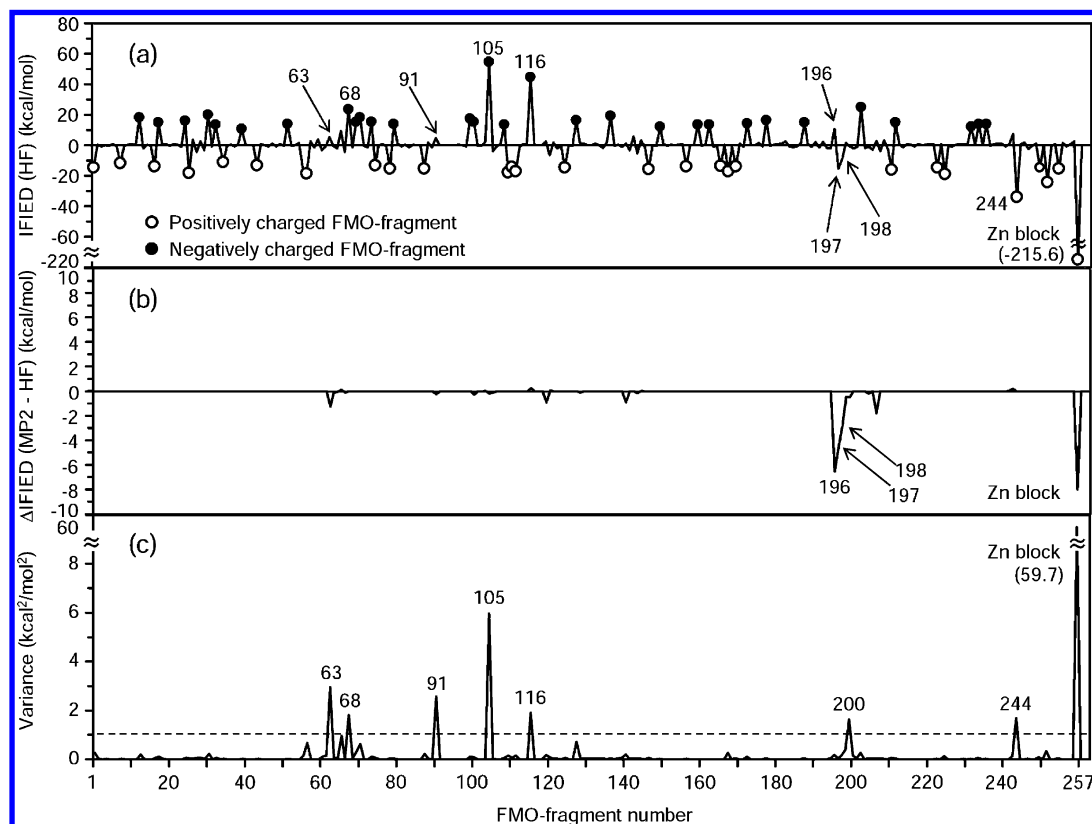


**Figure 4.** IFIED of BSA-bCA II complexes (a) IFIED of compound **6** ( $X = H$ ) with 257 FMO fragments in bCA II, calculated by HF/6-31G. (b) Difference between IFIEDs of compound **6**, calculated by MP2/6-31G and HF/6-31G. (c) Variance of IFIED among 16 BSA-bCA II complexes.

**Table 6.** Correlation Equations

$\Delta E_{\text{bind}} = aX + \text{constant} \quad (n = 16)$							
eq no.	$X$	$a^a$	constant <sup>a</sup>	$r^a$	$s^a$	$s_{\text{cv}}^a$	$F^a$
7	$\Sigma \text{IFIED}(i)$	$1.10 \pm 0.0907$	$8.95 \pm 10.0$	0.990	0.625	0.664	680
8	$\Sigma' \text{IFIED}(i)$	$0.951 \pm 0.0927$	$-4.47 \pm 10.6$	0.986	0.737	0.828	484
9	IFIED(Zn block)	$0.519 \pm 0.106$	$-4.57 \pm 22.1$	0.942	1.47	1.60	111

<sup>a</sup> See Table 5.

and positively charged FMO fragments (Arg and Lys), exhibiting attractive interaction energy. Like the IFIED values of the positively charged FMO fragments, IFIED(197) and IFIED(198) exhibit considerably large attractive interaction energies. The stabilization of IFIED(197) and IFIED(198) results from the hydrogen-bonding and/or electrostatic interactions of Thr197 and Thr198 with the sulfonamide group of BSA, as shown in Figure 2. As can be seen in Table 2, there is close contact between the negatively charged sulfonamide group and the two residues Thr197 and Thr198. The destabilization of IFIED(196) is due to the close steric contact between the side chain of Leu196 and the benzene ring of BSA. Those of IFIED(63) and IFIED(91) are due to the close contact of the para position (C4 in Figure 2) in the benzene ring of BSA with the side chain of His63 and that of the meta position (C5) with the side chain of Gln91, respectively.

Table 7 lists the  $\Sigma \text{IFIED}(i)$  values for the 16 complexes. FMO fragments exhibiting the great variance of IFIED are supposed to govern the variation of the total binding

energy. In fact, without large changes in the coefficient values of  $\Sigma \text{IFIED}(i)$  in eq 7,  $\Sigma \text{IFIED}(i)$  can be successfully replaced by the sum of selected IFIED values exhibiting the great variance. In eq 8,  $\Sigma' \text{IFIED}(i)$  denotes the sum of the IFIED values of the following eight FMO fragments exhibiting the variance greater than 1.0 kcal<sup>2</sup>/mol<sup>2</sup>: His63, Glu68, Gln91, Glu105, Glu116, Pro200, Arg244, and the Zn block (shown in Figure 4c and Table 7). Thus,  $\Delta E_{\text{bind}}$  is effectively expressed by the sum of the IFIED values of only these eight FMO fragments, which are located in the active site. It should be noted that Leu196, Thr197, and Thr198, which make the van der Waals contacts with BSAs and exhibit considerably large absolute IFIED values, are not responsible for the variation in  $\Delta E_{\text{bind}}$  because of their small IFIED variance.

The interaction of BSA with the Zn block, which exhibits the lowest interaction energy and the greatest variance among the selected FMO fragments used in eq 8, governs the variations in  $\Delta E_{\text{bind}}$ , as suggested by eq 9.



**Table 7.**  $\Delta E_{\text{bind}}$  and IFIED Values

compound			IFIED( <i>i</i> ) <sup>a</sup>												
no.	X	$\Delta E_{\text{bind}}^a$	$\Sigma$	$\Sigma'$	(63)	(68)	(91)	(105)	(116)	(196)	(197)	(198)	(200)	(244)	(Zn block)
1	4-CH <sub>3</sub> NH	-120.49	-117.70	-121.79	4.72	23.68	4.58	55.58	45.39	11.01	-15.34	-9.30	-2.07	-34.07	-219.60
2	4-NH <sub>2</sub>	-120.40	-117.44	-121.26	4.52	23.87	4.45	55.35	45.22	10.85	-15.25	-9.36	-1.91	-33.93	-218.82
3	4-CH <sub>3</sub> O	-116.46	-113.45	-117.22	4.34	22.88	4.90	55.06	44.95	10.70	-15.10	-9.79	0.86	-34.40	-215.81
4	4-CH <sub>3</sub>	-116.64	-113.89	-118.80	5.73	23.50	4.60	55.01	44.95	11.00	-15.37	-8.89	-1.60	-33.99	-217.00
5	3-CH <sub>3</sub>	-115.34	-112.43	-117.04	5.47	23.39	5.18	54.94	44.95	10.87	-15.33	-9.57	-0.62	-34.15	-216.20
6	H	-116.09	-113.09	-117.37	5.50	23.44	4.52	54.76	44.80	10.64	-15.31	-9.39	-0.78	-34.01	-215.60
6 <sup>b</sup>	H	-140.08	-141.68	-127.35	4.25	23.44	4.29	54.56	45.04	4.12	-19.90	-12.27	-1.26	-34.05	-223.62
7	4-Cl	-112.15	-109.45	-113.27	4.03	24.06	4.12	52.86	43.65	10.65	-15.14	-9.68	-0.07	-33.11	-208.81
8	4-Br	-111.95	-109.26	-113.13	3.98	24.06	4.12	52.90	43.67	10.66	-15.17	-9.58	-0.06	-33.12	-208.69
9	3-Cl	-111.66	-109.18	-113.38	4.94	24.88	4.47	52.65	43.67	10.99	-15.35	-9.36	-1.38	-32.78	-209.81
10	4-CH <sub>3</sub> CO	-112.24	-109.65	-113.25	1.01	23.18	5.05	53.43	44.01	10.20	-14.86	-9.83	2.49	-33.71	-208.70
11	4-CN	-108.92	-106.05	-109.84	3.25	24.56	4.13	51.30	42.73	10.98	-14.98	-9.54	-0.04	-32.26	-203.50
12	3-NO <sub>2</sub>	-111.14	-109.89	-112.03	3.96	26.90	1.18	50.23	42.47	11.22	-15.06	-9.24	-1.95	-31.26	-203.55
13	4-NO <sub>2</sub>	-109.52	-107.21	-108.30	1.39	25.72	1.23	50.61	42.56	9.80	-14.57	-10.00	1.44	-32.20	-199.06
14	3,4-di-Cl	-108.37	-106.23	-110.08	3.75	25.11	4.32	51.38	42.75	11.00	-15.11	-9.70	-0.51	-32.23	-204.65
15	3-NO <sub>2</sub> , 4-Cl	-109.50	-108.54	-110.49	2.81	27.29	-0.32	48.94	41.58	11.39	-15.06	-9.14	-1.25	-30.60	-198.95
16	3-CF <sub>3</sub> , 4-NO <sub>2</sub>	-105.95	-105.06	-107.65	-0.35	26.06	3.44	47.68	40.84	11.60	-14.93	-10.54	-0.12	-30.37	-194.83
variance <sup>c</sup>		18.07	14.56	19.42	2.96	1.81	2.56	5.97	1.89	0.18	0.05	0.15	1.63	1.67	59.67

<sup>a</sup> In kcal/mol. <sup>b</sup> MP2/6-31G. <sup>c</sup> In kcal<sup>2</sup>/mol<sup>2</sup>.

**3.4. Interpretation of Correlation between  $\Delta G$  and Hammett  $\sigma$ .** Kakeya et al.<sup>19–22</sup> and also Hansch et al.<sup>23,25</sup> found a significant correlation between the log (1/ $K_i$ ) value and the Hammett  $\sigma$  constant of a substituent in BSAs. The positive coefficient of  $\sigma$  in the correlation equation changes to a negative coefficient in the correlation equation involving  $\Delta G$  ( $=2.303RT \log K_i$ ). In fact,  $\Delta G$  exhibits a negative correlation with  $\sigma$  ( $r = -0.939$ ), indicating that an electron-withdrawing substituent such as 4-NO<sub>2</sub> stabilizes the overall complex formation process. The solvation and dissociation free energy contribution ( $\Delta G_{\text{sol}} + \Delta G_{\text{dis}}$ ) also shows a nice negative correlation with  $\sigma$  [ $r = -0.971$  ( $\Delta G_{\text{dis}}(\text{CPCM})$ ),  $-0.961$  ( $\Delta G_{\text{dis}}(\text{GB/SA-MO})$ )]. On the other hand, the intrinsic interaction energy ( $\Delta E_{\text{bind}}$ ) shows a nice, but positive correlation with  $\sigma$  ( $r = 0.969$ ), suggesting that an electron-donating substituent such as 4-NH<sub>2</sub> stabilizes the electrostatic interaction between Zn<sup>2+</sup> and the negatively charged sulfonamide groups in BSAs. These correlations indicate that ( $\Delta G_{\text{sol}} + \Delta G_{\text{dis}}$ ) and  $\Delta E_{\text{bind}}$  are both linearly correlated with  $\sigma$  and support the finding on SCRF, GB/SA, and FMO calculations; i.e., that the contribution from  $\Delta G_{\text{sol}} + \Delta G_{\text{dis}}$  governs  $\Delta G$  and it counteracts that of  $\Delta E_{\text{bind}}$ .

#### 4. CONCLUSIVE REMARKS

The present study is reasonably considered to show that the current approach using MD-GB/SA-FMO calculations is able to describe the quantitative free energy profile of complex formation between BSAs with bCA II. Analysis involving the FMO–IFIED terms quantitatively reveals the contribution of an individual amino acid residue in bCA II to the intrinsic interaction energy. It is noteworthy that the IFIED term attributable to the interaction energy of a ligand with a component amino acid residue in the protein, instead of the classical QSAR parameters attributable to a ligand, can be used as QSAR descriptors for analysis of the intrinsic interaction energy between BSAs and bCA II. In conclusion, the current approach provides quantitative information on the intrinsic interaction, solvation, and dissociation free energy contributions to the observed overall free energy

change accompanied by complex formation between BSAs and bCA II, which has not been obtainable with the classical QSAR.

#### ACKNOWLEDGMENT

This work was supported by the Japan Science and Technology Corp. (JST-CREST) and Grants-in-Aid for Scientific Research (No. 20590036) from the Ministry of Education, Culture, Sports, Science and Technology. We thank Professor Shigenori Tanaka (Kobe University, Japan), Professor Yuji Mochizuki (Rikkyo University, Japan), and Professor Toshio Fujita (Kyoto University, Japan) for their instructive suggestions.

#### REFERENCES AND NOTES

- (1) Lindskog, S. Carbonic Anhydrase. In *Zinc Enzymes*; Spiro, T. G., Ed.; John Wiley & Sons: New York, 1983; pp 78–121.
- (2) Lindskog, S. Structure and Mechanism of Carbonic Anhydrase. *Pharmacol. Ther.* **1997**, *74*, 1–20.
- (3) Supuran, C. T. Carbonic Anhydrase: Catalytic and Inhibition Mechanisms, Distribution and Physiological Roles. In *Carbonic Anhydrase: Its Inhibitors and Activators*; Supuran, C. T., Scozzafava, A., Conway, J., Eds.; CRC Press: Boca Raton, FL, 2004; pp 1–25.
- (4) Innocenti, A.; Antel, J.; Wurl, M.; Vullo, D.; Firmges, M. A.; Scozzafava, A.; Supuran, C. T. Carbonic Anhydrase Inhibitors. Inhibition of Isozymes I, II, IV, V and IX with Complex Fluorides, Chlorides and Cyanides. *Bioorg. Med. Chem. Lett.* **2005**, *15*, 1909–1913.
- (5) Nishimori, I.; Innocenti, A.; Vullo, D.; Scozzafava, A.; Supuran, C. T. Carbonic Anhydrase Inhibitors. Inhibition Studies of the Human Secretory Isoform VI with Anions. *Bioorg. Med. Chem. Lett.* **2007**, *17*, 1037–1042.
- (6) Nishimori, I.; Minakuchi, T.; Onishi, S.; Vullo, D.; Scozzafava, A.; Supuran, C. T. Carbonic Anhydrase Inhibitors. DNA Coning, Characterization, and Inhibition Studies of the Human Secretory Isoform VI, A New Target for Sulfonamide and Sulfamate Inhibitors. *J. Med. Chem.* **2007**, *50*, 381–388.
- (7) Wilkinson, B. L.; Innocenti, A.; Vullo, D.; Supuran, C. T.; Poulsen, S.-A. Inhibition of Carbonic Anhydrases with Glycosyltriazol Benzene Sulfonamides. *J. Med. Chem.* **2008**, *51*, 1945–1953.
- (8) D'Ambrosio, D.; Vitale, R.-M.; Dogné, J.-M.; Masereel, B.; Innocenti, A.; Scozzafava, A.; Simone, G. D.; Supuran, C. T. Carbonic Anhydrase Inhibitors: Bioreductive Nitro-Containing Sulfonamides with Selectivity for Targeting the Tumor Associated Isoforms IX and XII. *J. Med. Chem.* **2008**, *51*, 3230–3237.
- (9) Thiry, A.; Supuran, C. T.; Masereel, B.; Donge, J.-M. Recent Developments of Carbonic Anhydrase Inhibitors as Potential Anticancer Drugs. *J. Med. Chem.* **2008**, *51*, 3051–3056.
- (10) Supuran, C. T. Carbonic Anhydrases: Novel Therapeutic Applications for Inhibitors and Activators. *Nat. Rev. Drug Discovery* **2008**, *7*, 168–181.

- (11) Nair, S. K.; Krebs, J. B.; Christianson, D. W.; Fierke, C. A. Structural Basis of Inhibitor Affinity to Variants of Human Carbonic Anhydrase II. *Biochemistry* **1995**, *34*, 3981–3989.
- (12) Eriksson, A. E.; Jones, T. A.; Liljas, A. Refined Structure of Human Carbonic Anhydrase II at 2.0 Å Resolution. *Proteins* **1988**, *4*, 274–282.
- (13) Kim, C.-Y.; Chang, J. S.; Doyon, J. B.; Baird, T. T., Jr.; Fierke, C. A.; Jain, A.; Christianson, D. W. Contribution of Fluorine to Protein–Ligand Affinity in the Binding of Fluoroaromatic Inhibitors to Carbonic Anhydrase II. *J. Am. Chem. Soc.* **2000**, *122*, 12125–12134.
- (14) Saito, R.; Sato, T.; Ikai, A.; Tanaka, N. Structure of Bovine Carbonic Anhydrase II at 1.95 Å Resolution. *Acta Crystallogr., Sect. D: Biol. Crystallogr.* **2004**, *60*, 792–795.
- (15) Srivastava, D. K.; Jude, K. M.; Banerjee, A. L.; Haldar, M.; Manokaran, S.; Kooren, J.; Mallik, S.; Christianson, D. W. Structural Analysis of Charge Discrimination in the Binding of Inhibitors to Human Carbonic Anhydrases I and II. *J. Am. Chem. Soc.* **2007**, *129*, 5528–5537.
- (16) Temperini, C.; Cecchi, A.; Scozzafava, A.; Supuran, C. T. Carbonic Anhydrase Inhibitors. Comparison of Chlorthalidone and Indapamide X-ray Crystal Structures in Adducts with Isozyme II: When Three Water Molecules and the Keto–Enol Tautomerism Make the Difference. *J. Med. Chem.* **2009**, *52*, 322–328.
- (17) Scott, A. D.; Phillips, C.; Alex, A.; Flocco, M.; Bent, A.; Randall, A.; O'Brien, R.; Damian, L.; Jones, L. H. Thermodynamic Optimisation in Drug Discovery: A Case Study Using Carbonic Anhydrase Inhibitors. *Chem. Med. Chem.* **2009**, *4*, 1985–1989.
- (18) Supuran, C. T.; Casini, A.; Scozzafava, A. Development of Carbonic Anhydrase Inhibitors. In *Carbonic Anhydrase: Its Inhibitors and Activators*; Supuran, C. T., Scozzafava, A., Conway, J., Eds.; CRC Press: Boca Raton, FL, 2004; pp 67–148.
- (19) Kakeya, N.; Aoki, M.; Kamada, A.; Yata, N. Biological Activities of Drugs. VI. Structure–Activity Relationship of Sulfonamide Carbonic Anhydrase Inhibitors (1). *Chem. Pharm. Bull.* **1969**, *17*, 1010–1018.
- (20) Kakeya, N.; Yata, N.; Kamada, A.; Aoki, M. Biological Activities of Drugs. VII. Structure–Activity Relationship of Sulfonamide Carbonic Anhydrase Inhibitors (2). *Chem. Pharm. Bull.* **1969**, *17*, 2000–2007.
- (21) Kakeya, N.; Yata, N.; Kamada, A.; Aoki, M. Biological Activities of Drugs. VIII. Structure–Activity Relationship of Sulfonamide Carbonic Anhydrase Inhibitors (3). *Chem. Pharm. Bull.* **1969**, *17*, 2558–2564.
- (22) Kakeya, N.; Yata, N.; Kamada, A.; Aoki, M. Biological Activities of Drugs. VIII. Structure–Activity Relationship of Sulfonamide Carbonic Anhydrase Inhibitors (4). *Chem. Pharm. Bull.* **1970**, *18*, 191–194.
- (23) Hansch, C.; McClarin, J.; Klein, T.; Langridge, R. A Quantitative Structure–Activity Relationship and Molecular Graphics Study of Carbonic Anhydrase Inhibitors. *Mol. Pharmacol.* **1985**, *27*, 493–498.
- (24) Carotti, A.; Raguseo, C.; Campagna, F.; Langridge, R.; Klein, T. E. Inhibition of Carbonic Anhydrase by Substituted Benzenesulfonamides. A Reinvestigation by QSAR and Molecular Graphics Analysis. *Quant. Struct.–Act. Relat.* **1989**, *8*, 1–10.
- (25) Hansch, C. Comparative QSAR of the Sulfonamide Function. *Farmaco* **2003**, *58*, 625–629.
- (26) Benedetti, P. G. D.; Menziani, M. C.; Frassinetti, C. A Quantum Chemical QSAR Study of Carbonic Anhydrase Inhibition by Sulfonamides. Sulfonamide Carbonic Anhydrase Inhibitors: Quantum Chemical QSAR. *Quant. Struct.–Act. Relat.* **1985**, *4*, 23–28.
- (27) Benedetti, P. G. D.; Menziani, M. C.; Cocchi, M.; Frassinetti, C. A Quantum Chemical QSAR Analysis of Carbonic Anhydrase Inhibition by Heterocyclic Sulfonamides. Sulfonamide Carbonic Anhydrase Inhibitors: Quantum Chemical QSAR. *Quant. Struct.–Act. Relat.* **1987**, *6*, 51–53.
- (28) Menziani, M. C.; Benedetti, P. G. D. Molecular Mechanics and Quantum Chemical QSAR Analysis in Carbonic Anhydrase–Heterocyclic Sulfonamide Interactions. *Struct. Chem.* **1992**, *3*, 215–219.
- (29) Gupta, S. P.; Maheswaran, V.; Pande, V.; Kumar, D. A Comparative QSAR Study on Carbonic Anhydrase and Matrix Metalloproteinase Inhibition by Sulfonated Amino Acid Hydroxamates. *J. Enzyme Inhib. Med. Chem.* **2003**, *18*, 7–13.
- (30) Jaiswal, M.; Khadikar, P. V.; Scozzafava, A.; Supuran, C. T. Carbonic Anhydrase Inhibitors: The First QSAR Study on Inhibition of Tumor-Associated Isoenzyme IX with Aromatic and Heterocyclic Sulfonamides. *Bioorg. Med. Chem. Lett.* **2004**, *14*, 3283–3290.
- (31) Khadikar, P. V.; Sharma, V.; Karmarkar, S.; Supuran, C. T. QSAR Studies on Benzene Sulfonamide Carbonic Anhydrase Inhibitors: Need of Hydrophobic Parameter for Topological Modeling of Binding Constants of Sulfonamides to Human CA-II. *Bioorg. Med. Chem. Lett.* **2005**, *15*, 923–930.
- (32) Weber, A.; Böhm, M.; Supuran, C. T.; Scozzafava, A.; Sottriffer, C. A.; Klebe, G. 3D QSAR Selectivity Analyses of Carbonic Anhydrase Inhibitors: Insights for the Design of Isozyme Selective Inhibitors. *J. Chem. Inf. Model.* **2006**, *46*, 2737–2760.
- (33) Melagraki, G.; Afantitis, A.; Sarimveis, H.; Igglessi-Markopoulou, O.; Supuran, C. T. QSAR Study on *Para*-Substituted Aromatic Sulfonamides as Carbonic Anhydrase II Inhibitors Using Topological Information Indices. *Bioorg. Med. Chem.* **2006**, *14*, 1108–1114.
- (34) Clare, B. W.; Supuran, C. T. A Perspective on Quantitative Structure–Activity Relationships and Carbonic Anhydrase Inhibitors. *Expert Opin. Drug Metab. Toxicol.* **2006**, *2*, 113–137.
- (35) Eroğlu, E.; Türkmen, H.; Güler, S.; Palaz, S.; Öltulu, O. A. DFT-Based QSARs Study of Acetazolamide/Sulfanilamide Derivatives with Carbonic Anhydrase (CA-II) Isozyme Inhibitory Activity. *Int. J. Mol. Sci.* **2007**, *8*, 145–155.
- (36) Singh, S.; Khadikar, P. V.; Scozzafava, A.; Supuran, C. T. QSAR Studies for the Inhibition of the Transmembrane Carbonic Anhydrase Isozyme XIV with Sulfonamides Using PRECLAV Software. *J. Enzyme Inhib. Med. Chem.* **2009**, *24*, 337–349.
- (37) Gupta, S. P. Quantitative Structure–Activity Relationships of Carbonic Anhydrase Inhibitors. *Prog. Drug Res.* **2003**, *60*, 171–204.
- (38) Clare, B. W.; Supuran, C. T. QSAR Studies of Sulfonamide Carbonic Anhydrase Inhibitors. In *Carbonic Anhydrase: Its Inhibitors and Activators*; Supuran, C. T., Scozzafava, A., Conway, J., Eds.; CRC Press: Boca Raton, FL, 2004; pp 149–182.
- (39) Yoshida, T.; Yamagishi, K.; Chuman, H. QSAR Study of Cyclic Urea Type HIV-1 PR Inhibitors Using Ab Initio MO Calculation of Their Complex Structures with HIV-1 PR. *QSAR Comb. Sci.* **2008**, *27*, 694–703.
- (40) Yoshida, T.; Fujita, T.; Chuman, H. Novel Quantitative Structure–Activity Studies of HIV-1 Protease Inhibitors of the Cyclic Urea Type Using Descriptors Derived from Molecular Dynamics and Molecular Orbital Calculations. *Curr. Comput.-Aided Drug Des.* **2009**, *5*, 38–55.
- (41) Lindskog, S.; Thorslund, A. On the Interaction of Bovine Cobalt Carbonic Anhydrase with Sulfonamides. *Eur. J. Biochem.* **1968**, *3*, 453–460.
- (42) Kanamori, K.; Roberts, J. D. Nitrogen-15 Nuclear Magnetic Resonance Study of Benzenesulfonamide and Cyanate Binding to Carbonic Anhydrase. *Biochemistry* **1983**, *153*, 553–558.
- (43) Blackburn, G. M.; Mann, B. E.; Taylor, B. F.; Worrall, A. F. A Nuclear-Magnetic-Resonance Study of the Binding of Novel *N*-Hydroxybenzenesulphonamide Carbonic Anhydrase Inhibitors to Native and Cadmium-111-Substituted Carbonic Anhydrase. *Eur. J. Biochem.* **1985**, *153*, 553–558.
- (44) Koike, T.; Kimura, E.; Nakamura, I.; Hashimoto, Y.; Shiro, M. The First Anionic Sulfonamide-Binding Zinc(II) Complexes with a Macrocyclic Triamine: Chemical Verification of the Sulfonamide Inhibition of Carbonic Anhydrase. *J. Am. Chem. Soc.* **1992**, *114*, 7338–7345.
- (45) Krishnamurthy, V. M.; Kaufman, G. K.; Urbach, A. R.; Gitlin, I.; Gudiksen, K. L.; Weibel, D. B.; Whitesides, G. M. Carbonic Anhydrase as a Model for Biophysical and Physical–Organic Studies of Proteins and Protein–Ligand Binding. *Chem. Rev.* **2008**, *108*, 946–1051.
- (46) Krishnamurthy, V. M.; Bohall, B. R.; Kim, C.-Y.; Moustakas, D. T.; Christianson, D. W.; Whitesides, G. M. Thermodynamic Parameters for the Association of Fluorinated Benzenesulfonamides with Bovine Carbonic Anhydrase II. *Chem. Asian J.* **2007**, *2*, 94–105.
- (47) Merz, K. M., Jr.; Murcko, M. A.; Kollman, P. A. Inhibition of Carbonic Anhydrase. *J. Am. Chem. Soc.* **1991**, *113*, 4484–4490.
- (48) Noskov, S. V.; Lim, C. Free Energy Decomposition of Protein–Protein Interactions. *Biophys. J.* **2001**, *81*, 737–750.
- (49) Massova, I.; Kollman, P. A. Computational Alanine Scanning to Probe Protein–Protein Interactions: A Novel Approach To Evaluate Binding Free Energies. *J. Am. Chem. Soc.* **1999**, *121*, 8133–8143.
- (50) Froloff, N.; Windemuth, A.; Honig, B. On the Calculation of Binding Free Energies Using Continuum Methods: Application to MHC Class I Protein–Peptide Interactions. *Protein Sci.* **1997**, *6*, 1293–1301.
- (51) Barreiro, G.; Guimaraes, C. R. W.; Tubert-Brohman, I.; Lyons, T. M.; Tirado-Rives, J.; Jorgensen, W. L. Search for Non-nucleoside Inhibitors of HIV-1 Reverse Transcriptase Using Chemical Similarity, Molecular Docking, and MM-GB/SA Scoring. *J. Chem. Inf. Model.* **2007**, *47*, 2416–2428.
- (52) Kallies, B.; Mitzner, R. Substrate Specificity of Chymotrypsin. Study of Induced Strain by Molecular Mechanics. *J. Mol. Model.* **1996**, *2*, 149–159.
- (53) Jayaram, B.; McConnell, K.; Dixit, S. B.; Das, A.; Beveridge, D. L. Free-Energy Component Analysis of 40 Protein–DNA Complexes: A Consensus View on the Thermodynamics of Binding at the Molecular Level. *J. Comput. Chem.* **2002**, *23*, 1–14.
- (54) Dullweber, F.; Stubbs, M. T.; Musil, D.; Sturzebecher, J.; Klebe, G. Factorising Ligand Affinity: A Combined Thermodynamic and Crystallographic Study of Trypsin and Thrombin Inhibition. *J. Mol. Biol.* **2001**, *313*, 593–614.
- (55) Czodrowski, P.; Sottriffer, C. A.; Klebe, G. Protonation Changes upon Ligand Binding to Trypsin and Thrombin: Structural Interpretation Based on pK<sub>a</sub> Calculations and ITC Experiments. *J. Mol. Biol.* **2007**, *367*, 1347–1356.



- (56) Naim, M.; Bhat, S.; Rankin, K. N.; Dennis, S.; Chowdhury, S. F.; Siddiqi, I.; Drabik, P.; Sulea, T.; Bayly, C. I.; Jakalian, A.; Purisima, E. O. Solvated Interaction Energy (SIE) for Scoring Protein–Ligand Binding Affinities. I. Exploring the Parameter Space. *J. Chem. Inf. Model.* **2007**, *47*, 122–133.
- (57) Gohlke, H.; Klebe, G. Statistical Potentials and Scoring Functions Applied to Protein–Ligand Binding. *Curr. Opin. Struct. Biol.* **2001**, *11*, 231–235.
- (58) Morris, G. M.; Goodsell, D. S.; Halliday, R. S.; Huey, R.; Hart, W. E.; Belew, R. K.; Olson, A. J. Automated Docking Using a Lamarckian Genetic Algorithm and an Empirical Binding Free Energy Function. *J. Comput. Chem.* **1998**, *19*, 1639–1662.
- (59) Oprea, T. I.; Marshall, G. R. Receptor-Based Prediction of Binding Affinities. In *3D QSAR in Drug Design*; Kubyini, H., Folkers, G., Martin, Y., Eds.; Kluwer/Escom: Dordrecht, The Netherlands, 1998; pp 35–61.
- (60) Jones-Hertzog, D. K.; Jorgensen, W. L. Binding Affinities for Sulfonamide Inhibitors with Human Thrombin Using Monte Carlo Simulations with a Linear Response Method. *J. Med. Chem.* **1997**, *40*, 1539–1549.
- (61) Tominaga, Y.; Jorgensen, W. L. General Model for Estimation of the Inhibition of Protein Kinases Using Monte Carlo Simulations. *J. Med. Chem.* **2004**, *47*, 2534–2549.
- (62) Freire, E. A. Thermodynamic Approach to the Affinity Optimization of Drug Candidates. *Chem. Biol. Drug Des.* **2009**, *74*, 468–472.
- (63) Grunwald, E. Enthalpy–Entropy Compensation and Solvent Reorganization. In *Drug–Receptor Thermodynamics: Introduction and Applications*; Raffa, R. B., Ed.; Wiley: Chichester, U.K., 2001; pp 553–573.
- (64) Exner, O. Entropy–Enthalpy Compensation and Anticompensation: Solvation and Ligand Binding. *Chem. Commun. (Cambridge, U.K.)* **2000**, 1655–1656.
- (65) Frederick, K. K.; Marlow, M. S.; Valentine, K. G.; Wand, A. J. Conformational Entropy in Molecular Recognition by Proteins. *Nature* **2007**, *448*, 325–329.
- (66) Kinoshita, M.; Harano, Y.; Akiyama, R. Changes in Thermodynamic Quantities upon Contact of Two Solutes in Solvent under Isochoric and Isobaric Conditions. *J. Chem. Phys.* **2006**, *125*, 224504–1–224504–7.
- (67) Fialkov, Y. Y.; Gorbachev, V. Y.; Kamenskaya, T. A. Thermodynamic Characteristics of the Ionic Association Process of Acids in Aqueous Solution. *J. Mol. Liq.* **2003**, *102*, 277–284.
- (68) Matsui, T.; Ko, H. C.; Hepler, L. G. Thermodynamics of Ionization of Benzoic Acid and Substituted Benzoic Acids in Relation to the Hammett Equation. *Can. J. Chem.* **1974**, *52*, 2906–2911.
- (69) Grünberg, R.; Nilges, M.; Leckner, J. Flexibility and Conformational Entropy in Protein–Protein Binding. *Structure* **2006**, *14*, 683–93.
- (70) Fedorov, D. G.; Kitaura, K. Extending the Power of Quantum Chemistry to Large Systems with the Fragment Molecular Orbital Method. *J. Phys. Chem. A* **2007**, *111*, 6904–6914.
- (71) Zou, X.; Sun, Y.; Kuntz, I. D. Inclusion of Solvation in Ligand Binding Free Energy Calculations Using the Generalized-Born Model. *J. Am. Chem. Soc.* **1999**, *121*, 8033–8043.
- (72) Massova, I.; Kollman, P. A. Combined Molecular Mechanical and Continuum Solvent Approach (MM-PBSA/GBSA) to Predict Ligand Binding. *Perspect. Drug Discovery* **2000**, *18*, 113–135.
- (73) Tomasi, J.; Mennucci, B.; Cammi, R. Quantum Mechanical Continuum Solvation Models. *Chem. Rev.* **2005**, *105*, 2999–3093.
- (74) Cramer, C. J.; Truhlar, D. G. Implicit Solvation Models: Equilibria, Structure, Spectra, and Dynamics. *Chem. Rev.* **1999**, *99*, 2161–2200.
- (75) Hoops, S. C.; Anderson, K. W.; Merz, K. M., Jr. Force Field Design for Metalloproteins. *J. Am. Chem. Soc.* **1991**, *113*, 8262–8270.
- (76) Ryde, U. Molecular Dynamics Simulations of Alcohol Dehydrogenase with a Four- or Five-Coordinate Catalytic Zinc Ion. *Proteins* **1995**, *21*, 40–56.
- (77) Frisch, M. J.; Trucks, G. W.; Schlegel, H. B.; Scuseria, G. E.; Robb, M. A.; Cheeseman, J. R.; Montgomery, J. A., Jr.; T. V.; Kudin, K. N.; Burant, J. C.; Millam, J. C.; Iyengar, S. S.; Tomasi, J.; Barone, V.; Mennucci, B.; Cossi, M.; Scalmani, G.; Rega, N.; Petersson, G. A.; Nakatsuji, H.; Hada, M.; Ehara, M.; Toyota, K.; Fukuda, R.; Hasegawa, J.; Ishida, M.; Nakajima, T.; Honda, Y.; Kitao, O.; Nakai, H.; Klene, M.; Li, X.; Knox, J. E.; Hratchian, H. P.; Cross, J. B.; Adamo, C.; Jaramillo, J.; Gomperts, R.; Stratmann, R. E.; Yazyev, O.; Austin, A. J.; Cammi, R.; Pomelli, C.; Ochterski, J. W.; Ayala, P. Y.; Morokuma, K.; Voth, G. A.; Salvador, P.; Dannenberg, J. J.; Zakrzewski, G.; Dapprich, S.; Daniels, A. D.; Strain, M. C.; Farkas, O.; Malick, D. K.; Rabuck, A. D.; Raghavachari, K.; Foresman, J. B.; Ortiz, J. V.; Cui, Q.; Baboul, A. G.; Clifford, S.; Cioslowski, J.; Stefanov, B. B.; Liu, G.; Liashenko, A.; Piskorz, P.; Komaromi, I.; Martin, R. L.; Fox, D. J.; Keith, T.; Al-Laham, M. A.; Peng, C. Y.; Nanayakkara, A.; Challacombe, M.; Gill, P. M. W.; Johnson, B.; Chen, W.; Wong, M. W.; Gonzalez, C.; Pople, J. A. *Gaussian 03*, Revision D.02; Gaussian: Pittsburgh, PA, 2003.
- (78) Toba, S.; Colombo, G.; Merz, K. M., Jr. Solvent Dynamics and Mechanism of Proton Transfer in Human Carbonic Anhydrase II. *J. Am. Chem. Soc.* **1999**, *121*, 2290–2302.
- (79) Suárez, D.; Merz, K. M., Jr. Molecular Dynamics Simulations of the Mononuclear Zinc– $\beta$ -Lactamase from *Bacillus Cereus*. *J. Am. Chem. Soc.* **2003**, *123*, 3759–3770.
- (80) Bayly, C. I.; Cieplak, P.; Cornell, W. D.; Kollman, P. A. A Well Behaved Electrostatic Potential Based Method Using Charge Restraints for Deriving Atomic Charges: The RESP Model. *J. Phys. Chem.* **1993**, *97*, 10269–10280.
- (81) Case, D. A.; Cheatham, T. E., III; Darden, T.; Gohlke, H.; Luo, R.; Merz, K. M., Jr.; Onufriev, A.; Simmerling, C.; Wang, B.; Woods, R. J. The Amber Biomolecular Simulation Programs. *J. Comput. Chem.* **2005**, *26*, 1668–1688.
- (82) Ryckaert, J. P.; Cicotti, G.; Berendsen, H. J. C. Numerical Integration of the Cartesian Equations of Motion of a System with Constraints: Molecular Dynamics of N-Alkanes. *J. Comput. Phys.* **1977**, *23*, 327–341.
- (83) Darden, T. A.; York, D. M.; Pedersen, L. G. Particle Mesh Ewald—An  $N \cdot \log(N)$  Method for Ewald Sums in Large Systems. *J. Chem. Phys.* **1993**, *98*, 10089–10092.
- (84) Shao, J.; Tanner, S. W.; Thompson, N.; Cheatham, T. E. III. Clustering Molecular Dynamics Trajectories: I. Characterizing the Performance of Different Clustering Algorithms. *J. Chem. Theory Comput.* **2007**, *3*, 2312–2334.
- (85) Svensson, M.; Humbel, S.; Froese, R. D. J.; Matsubara, T.; Sieber, S.; Morokuma, K. ONIOM: A Multilayered Integrated MO + MM Method for Geometry Optimizations and Single Point Energy Predictions. A Test for Diels–Alder Reactions and  $\text{Pt}(\text{P}(\text{t-Bu})_3)_2 + \text{H}_2$  Oxidative Addition. *J. Phys. Chem.* **1996**, *100*, 19357–19363.
- (86) Torrent, M.; Vreven, T.; Musaev, D. G.; Morokuma, K.; Farkas, Ö.; Schlegel, H. B. Effects of the Protein Environment on the Structure and Energetics of Active Sites of Metalloenzymes. ONIOM Study of Methane Monooxygenase and Ribonucleotide Reductase. *J. Am. Chem. Soc.* **2002**, *124*, 192–193.
- (87) Lundberg, M.; Morokuma, K. Protein Environment Facilitates  $\text{O}_2$  Binding in Non-Heme Iron Enzyme. An Insight from ONIOM Calculations on Isopenicillin N Synthase (IPNS). *J. Phys. Chem. B* **2007**, *111*, 9380–9389.
- (88) Vreven, T.; Byun, K. S.; Komromi, I.; Dapprich, S.; Montgomery, J. A.; Morokuma, K.; Frisch, M. J. Combining Quantum Mechanics Methods with Molecular Mechanics Methods in ONIOM. *J. Chem. Theory Comput.* **2006**, *2*, 815–826.
- (89) Alterio, V.; De Simone, G.; Monti, S. M.; Scozzafava, A.; Supuran, C. T. Carbonic Anhydrase Inhibitors: Inhibition of Human, Bacterial, and Archaeal Isozymes with Benzene-1,3-Disulfonamides—Solution and Crystallographic Studies. *Bioorg. Med. Chem. Lett.* **2007**, *17*, 4201–4207.
- (90) Bashford, D.; Case, D. A. Generalized Born Models of Macromolecular Solvation Effects. *Annu. Rev. Phys. Chem.* **2000**, *51*, 129–152.
- (91) Cossi, M.; Rega, N.; Scalmani, G.; Barone, V. Energies, Structures, and Electronic Properties of Molecules in Solution with the C-PCM Solvation Model. *J. Comput. Chem.* **2003**, *24*, 669–681.
- (92) Barone, V.; Cossi, M.; Tomasi, J. A New Definition of Cavities for the Computation of Solvation Free Energies by the Polarizable Continuum Model. *J. Chem. Phys.* **1997**, *107*, 3210–3221.
- (93) Liptak, M. D.; Shields, G. C. Accurate  $pK_a$  Calculations for Carboxylic Acids Using Complete Basis Set and Gaussian-n Models Combined with CPCM Continuum Solvation Methods. *J. Am. Chem. Soc.* **2001**, *123*, 7314–7319.
- (94) Sadlej-Sosnowska, N. Calculation of Acidic Dissociation Constants in Water: Solvation Free Energy Terms. Their Accuracy and Impact. *Theor. Chem. Acc.* **2007**, *118*, 281–293.
- (95) Watanabe, T.; Inadomi, Y.; Fukuzawa, K.; Nakano, T.; Tanaka, S.; Nilsson, L.; Nagashima, U. DNA and Estrogen Receptor Interaction Revealed by Fragment Molecular Orbital Calculations. *J. Phys. Chem. B* **2007**, *111*, 9621–9627.
- (96) Nakano, T.; Mochizuki, Y.; Kato, A.; Fukuzawa, K.; Ishikawa, T.; Amari, S.; Kurisaki, I.; Tanaka, S. Developments of FMO Methodology and Graphical User Interface in ABINIT-MP. In *The Fragment Molecular Orbital Method: Practical Applications to Large Molecular Systems*; Fedorov, D. G., Kitaura, K., Eds.; CRC Press: Boca Raton, FL, 2009; pp 37–59.
- (97) Nakanishi, I.; Fedorov, D. G.; Kitaura, K. Detailed Electronic Structure Studies Revealing the Nature of Protein–Ligand Binding. In *The Fragment Molecular Orbital Method: Practical Applications to Large Molecular Systems*; Fedorov, D. G., Kitaura, K., Eds.; CRC Press: Boca Raton, FL, 2009; pp 171–192.